AIMS Biophysics, 3(2): 247-260.
DOI: 10.3934/biophy.2016.2.247
Received: 14 March 2016
Accepted: 17 May 2016
Published: 18 May 2016

http://www.aimspress.com/journal/biophysics

Research article

Glycation and secondary conformational changes of human serum albumin: study of the FTIR spectroscopic curve-fitting technique

Yu-Ting Huang [1,2], Hui-Fen Liao [2], Shun-Li Wang [3], and Shan-Yang Lin [1,*]

[1] Department of Biotechnology and Pharmaceutical Technology, Yuanpei University of Medical Technology, Hsin Chu, Taiwan, ROC
[2] Department of Biochemical Science and Technology, National Chiayi University, Chiayi, Taiwan, ROC
[3] Department of Applied Chemistry, National Chiayi University, Chiayi, Taiwan, ROC

* **Correspondence:** E-mail: sylin@mail.ypu.edu.tw; Tel: +886-3-6102439; Fax: +886-3-6102328.

Abstract: The aim of this study was attempted to investigate both the glycation kinetics and protein secondary conformational changes of human serum albumin (HSA) after the reaction with ribose. The browning and fluorescence determinations as well as Fourier transform infrared (FTIR) microspectroscopy with a curve-fitting technique were applied. Various concentrations of ribose were incubated over a 12-week period at 37 ± 0.5 ^{o}C under dark conditions. The results clearly shows that the glycation occurred in HSA-ribose reaction mixtures was markedly increased with the amount of ribose used and incubation time, leading to marked alterations of protein conformation of HSA after FTIR determination.

In addition, the browning intensity of reaction solutions were colored from light to deep brown, as determined by optical observation. The increase in fluorescence intensity from HSA–ribose mixtures seemed to occur more quickly than browning, suggesting that the fluorescence products were produced earlier on in the process than compounds causing browning. Moreover, the predominant α-helical composition of HSA decreased with an increase in ribose concentration and incubation time, whereas total β-structure and random coil composition increased, as determined by curve-fitted FTIR microspectroscopy analysis. We also found that the peak intensity ratios at 1044 cm^{-1}/1542 cm^{-1} markedly decreased prior to 4 weeks of incubation, then almost plateaued, implying that the consumption of ribose in the glycation reaction might have been accelerated over the first 4 weeks of incubation, and gradually decreased. This study first evidences that two unique IR peaks at 1710 cm^{-1} [carbonyl groups of irreversible products produced by the reaction and

deposition of advanced glycation end products (AGEs)] and 1621 cm^{-1} (aggregated HSA molecules) were clearly observed from the curve-fitted FTIR spectra of HSA-ribose mixtures over the course of incubation time. This study clearly suggests that FTIR spectroscopic curve-fitting technique may be easily used to allow determining the marked changes in the secondary conformational structure and protein aggregation of HSA during ribosylation as well as the production of AGEs.

Keywords: human serum albumin (HSA); ribose; ribosylation; FTIR; curve-fitting; browning; fluorescence; protein aggregation; AGEs

1. Introduction

Advanced glycation end products (AGEs) have received considerable attention since glycation can easily occur both outside (exogenously) and inside (endogenously) the body [1]. AGEs can be exogenously formed during food preparation by heating [2,3], whereas an endogenous glycation reaction is easily triggered by the interaction between a carbohydrate and a protein without the involvement of an enzyme. AGEs slowly accumulate *in vivo* and make cells stiffer, i.e. less pliable and more prone to damage and premature aging caused by protein dysfunction [4–6]. Nowadays, a number of studies have confirmed that AGEs are associated with the development or worsening of many degenerative diseases such as cataracts, diabetes, atherosclerosis, chronic renal failure, Parkinson's disease, Alzheimer's disease, and amyotrophic lateral sclerosis [7–9]. The process of glycation starts with the formation of a Schiff base, followed by Amadori products, and various intermediate compounds are then produced, followed by the eventual formation of AGEs; this process is also referred as nonenzymatic glycosylation or the Maillard reaction [4,10,11]. Thus, the study of AGEs has become one of the most important areas of biochemistry today.

It is well known that all reducing sugars can participate in the glycation reaction in combination with various amino acids [12,13]. Sugar type is one of the numerous factors affecting the rate of the Maillard reaction, with pentoses having been found to be more reactive than hexoses. The glycating ability of reducing sugars was found to increase in the following order: D-glucose < D-mannose < D-galactose < D-xylose < D-fructose < D-arabinose < D-ribose [14,15]. Among these reducing sugars, D-ribose is the most reactive in the glycation of proteins and results in a more rapid production of AGEs than other sugars *in vitro* and *in vivo* [16–18].

Recently, the glycation of proteins with ribose (ribosylation) has attracted more attention due to protein aggregation and fibrillation, and the generation of reactive oxygen species (ROS) [15, 19–21]. However, several controversial results have led to a debate on whether glycation or ribosylation alters the protein conformational structure [21–24]. For this reason, ribosylation needs to be further investigated by evaluating the protein secondary conformational structure changes caused by the reaction.

In the present study, human serum albumin (HSA) was used as a model protein. It has been extensively used as a model for protein-folding and ligand-binding studies because it is the most abundant protein constituent of blood plasma in the human body [25,26]. There has also been much focus on the effects of glycation on the structure of HSA [27,28], which is divided into three homologous helical domains in which each domain is further subdivided into two subdomains with a

common helical motif [29]. Nonenzymatic glycation of HSA may affect its protein binding properties, thus resulting in abnormal biological effects [30], and many studies have indicated conformational changes of HSA after drug–protein binding [31]. In our previous studies, the effects of ethanol and/or captopril on the secondary structure of HSA before and after protein binding were investigated by Fourier transform infrared (FTIR) microspectroscopy [32,33]. Disulfide formation and secondary conformational changes in a captopril–HSA mixture after UV-B irradiation were also detected [34]. In this study, we attempt to examine the secondary conformational structure of HSA molecules after ribosylation using transmission FTIR microspectroscopy. UV absorbance, browning, and fluorescence development of Maillard reaction products (MRPs) in the HSA–ribose system were also determined.

2. Materials and Methods

2.1. Materials

Human serum albumin (HSA), D-ribose, and deuterium oxide (D_2O) were purchased from Sigma-Aldrich Co. LLC. (St. Louis, MO, USA) and used as supplied without further purification. All the reagents were of analytical grade and were also obtained from Sigma-Aldrich Co. LLC. The potassium bromide (KBr) crystals for the pellets were obtained from Jasco Parts Center (Jasco Co., Tokyo, Japan).

2.2. In vitro glycation of HSA with ribose

The glycation reaction of HSA with ribose was performed using a modification of the Sadowska–Bartosz method detailed in our previous studies [30–32,35].

HSA (50 mg/mL) was previously dissolved in D_2O with 0.03% sodium azide and incubated with different concentrations of ribose (10–200 mM) for 12 weeks at 37 ± 0.5 ^{o}C under dark conditions. At pre-defined intervals, the incubated solution was sampled for the following investigations.

(a) Measurement of nonenzymatic browning intensity of the samples using a UV/visible spectrophotometer (Cary 50 Conc., Varian**,** Australia) at 420 nm [36,37].
(b) Observation of color images of samples using a digital camera.
(c) Since ribose had been reported to be a strong inducer of fluorescence at 370 nm excitation and 440 nm emission [38], thus in this study the fluorescence intensities of HSA and HSA-ribose mixtures were determined using a fluorescence spectrophotometer (F-4500, Hitachi, Japan) by setting at 370 nm excitation and 440 nm emission.
(d) Measurement of the secondary conformational structure of HSA by FTIR microspectroscopy (IRT-5000-16/FTIR-6200, Jasco Co., Tokyo, Japan) using a film method on a calcium fluoride (CaF_2) plate via a transmission technique [39].

2.3. FTIR data acquisition and handling

The software, Spectral Manager for Windows (Jasco Co., Tokyo, Japan) and GRAMS spectroscopy software suite (Version 7, Thermo Electron Co., MA, USA), were used for data

acquisition and handling. The basic principle of curve fitting was to reconstruct the original amide I spectrum, then the baseline was first corrected from 1600–1700 cm^{-1}, followed secondary derivative. The number of bands and positions were taken from their second derivative spectra. Second derivative spectral analysis was previously applied to locate the position of the overlapping components in the amide I band and assigned to different secondary structures. Then these peaks obtained in the secondary derivatives were used for the curve fitting. The protein secondary structure and the composition of each component in the amide I band of the IR spectra were quantitatively estimated by a least-squares fitting program iterating the curve-fitting process using a Gaussian function. In the fitting process, the heights, widths, and positions of all bands were varied simultaneously. The rationale of any curve fitting procedure was to minimize the differences between the experimental absorption spectrum and the fitted spectrum. The curve fitting was performed by stepwise iterative adjustment towards minimum standard errors of the different parameters determining the shape and position of the absorption peaks. Finally, the proportion of a component was computed to be the fractional area of the corresponding peak divided by the sum of the areas of all the peaks [32–34].

2.4. Statistical analysis

All the tests were conducted in triplicate, and mean values with standard deviations were obtained. The significance of the differences between variables was determined using one-way analysis of variance (ANOVA).

3. Results and Discussion

3.1. Extent of browning intensity and color appearance

It is well known that the Maillard reaction may result in the formation of final browning compounds due to an advanced glycation reaction, so the UV absorbance and browning of MRPs were measured by UV spectroscopy using several reported methods [36,37]. The absorbance values (A_{420}) at 420 nm were used as an indicator of browning development in the final stage of the browning reaction. Figure 1-A shows the change in browning intensity of HSA–ribose mixtures during the 12-week incubation period. It clearly indicates that the browning intensity, measured as A_{420} values of the HSA–ribose mixtures, markedly increased with the concentration of ribose and the incubation time; the higher the concentration of ribose used, the higher the increase in A_{420} values ($p < 0.05$). In comparison, there were no changes for HSA or ribose alone ($p > 0.05$). The reaction mixture formed a gel after 6 weeks at the highest concentration of ribose used (50 mM), and further continuous measurement of UV absorption levels of the gelled samples could no longer be performed by UV spectroscopy. In addition, a large increase in the browning absorbance at 420 nm seems to be exponentially enhanced for the higher concentrations of ribose used in the course of incubation period.

The total color changes of the HSA aqueous solutions after the reaction with or without ribose were visibly observed, and the results are shown in Figure 1-B. Obviously, the reaction solutions colored from light to deep brown, suggesting that the Maillard reaction had occurred between the amino acids of HSA and the reactive reducing moieties of ribose. Compared with other sugars such

as glucose and fructose, ribose was the most strongly glycative molecule to cause the browning reaction indicating glycation (data not shown), which is consistent with results from other studies [14,15]. Moreover, the rate of glycation was also dependent on the type and concentration of monosaccharide [24,40,41]. The highest glycating capability of ribose might be due to its planar structure causing the unstable aldofuranose ring to react with the amino groups [24].

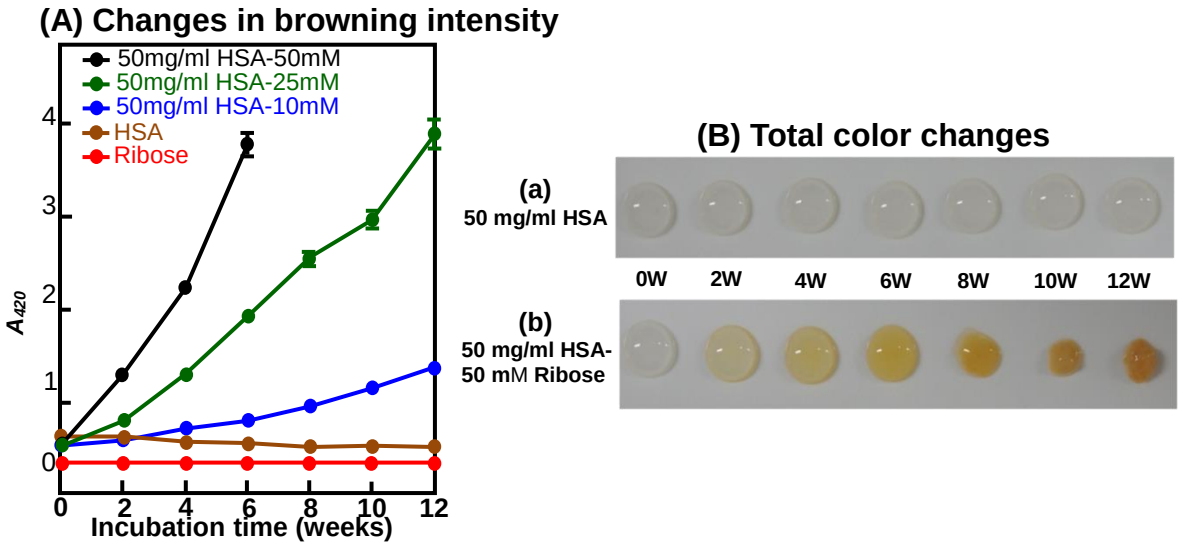

Figure 1. The changes in browning intensity (A) and total color appearance (B) of HSA-ribose mixtures over the course of 12 weeks of incubation.

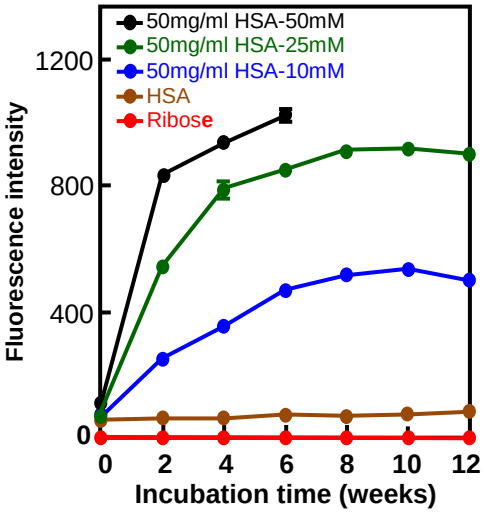

Figure 2. The changes in fluorescence intensity of HSA-ribose mixtures over the course of 12 weeks of incubation.

3.2. Changes in fluorescence intensity

AGEs are highly heterogeneous compounds classified into two major groups: fluorescent/crosslinking structures and non-fluorescent/ non-crosslinking structures [42]. We only investigated the total fluorescence of HSA-ribose mixtures using a fluorescence spectrophotometer in the present study. The results indicate that the fluorescence of the resulting mixtures increased with

the length of incubation time, as shown in Figure 2. It is evident that the fluorescence intensity of HSA–ribose mixtures rapidly increased with the amount of ribose used and incubation time. Moreover, the increased fluorescence intensity was also dependent on the ribose concentration used; the higher the concentration of ribose used, the more rapidly the fluorescence was observed. After incubation for 6–8 weeks, the fluorescence had almost reached a plateau, and over this period, the increase in the fluorescence intensity of the HSA–ribose mixtures seemed to occur more quickly than for browning. This might be because the fluorescent products were produced earlier on in the reaction than the browning compound, which is consistent with the results of Kato et al. [43]. In addition, the faster rate of fluorescence generation for nonenzymatically glycated HSA was possibly related to a faster conversion of the Amadori groups, similar to that of the glycation/fructation of bovine serum albumin or HSA [44,45].

3.3. Secondary structure alterations of HSA after ribosylation

Nonenzymatic glycation leads to the formation of inter- and intramolecular cross-links in proteins. This reaction not only modifies the conformation of proteins but also induces altered biological activity [46]. Since albumin has been reported to be highly susceptible to nonenzymatic glycation [27,47], it is of interest to determine the structural alterations in HSA modified by glycation. In order to detect the glycation-induced changes in protein conformation, several targets have been focused on in studies of the products of glycosylation reactions or of changes in either protein or sugar structure using various methods [48–50]. In the present study, we used transmission FTIR microspectroscopy with a curve-fitting technique to investigate the secondary conformational changes of glycated HSA.

Figure 3 shows the representative FTIR spectra of native HSA, ribose, and HSA–ribose (50 mg/mL/50 mM) using a film method on a CaF_2 plate via a transmission FTIR technique. The FTIR spectra of all samples in the wave amplitude range between 3800–2200 and 1800–800 cm^{-1} were examined. The characteristic IR absorption bands and their assignments for native HSA are as follows (in cm^{-1}): 3303 (amide A, N-H stretching), 2960 (C-H stretching), 1654 (amide I, C=O stretching), 1542 (amide II, C-N stretching and N-H bending), 1464 ($C-H_2$ bending), 1398 (carboxylate) and 1311–1247 cm^{-1} (Amide III, C-N stretching and N-H bending) [51]. For native HSA, the bands between 1500 and 1000 cm^{-1} are in the“fingerprint”region. On the other hand, the FTIR spectrum of ribose shows strong peaks between 1200 and 1000 cm^{-1}. Both peaks at 1085 and 1042 cm^{-1} can be used to distinguish the presence of ribose attached to HSA. The bands at 3369 and 2933 cm^{-1} are assigned to the CH and OH vibrational groups of ribose. The bands found in the 1200–1000 cm^{-1} range correspond to C-O and C-C stretching vibrations and the C-OH and C-C-O bending vibrations of ribose [52]. Once ribose was mixed with HSA at the initial stage, the FTIR spectrum of the HSA–ribose mixture was only superimposed by the FTIR spectra of HSA and ribose. Two marked FTIR peaks at 1088 and 1044 cm^{-1} were due to ribose, except the FTIR peaks belonging to HSA.

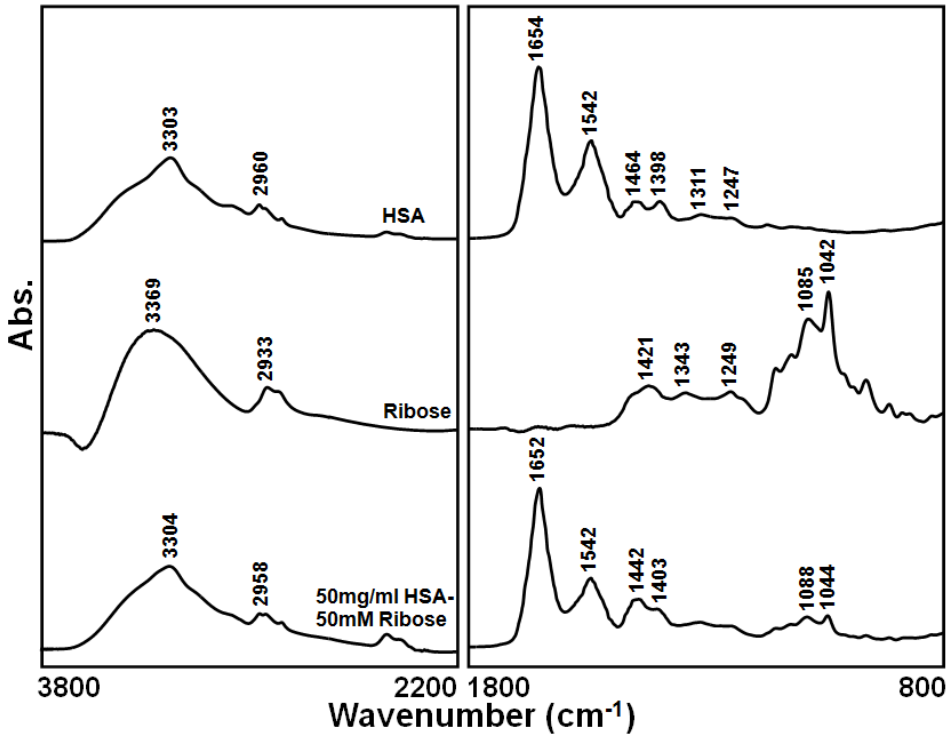

Figure 3. Representative FTIR spectra of native HSA, ribose, and HSA-ribose (50 mg/ml/50 mM) determined by a film method on a CaF_2 plate via transmission FTIR.

Although the specific stretching and bending vibrations of the peptide backbone in amide I, II, and III bands may provide information on various types of secondary structure, it is well known that the amide I band is particularly sensitive to protein secondary structure changes than the others [51,53]. Figure 4 shows the curve-fitted amide I band of HSA with and without the addition of ribose at the initial stage; the curve-fitted amide I bands of both HSA samples and their components, assignments, and compositions are illustrated. The results clearly indicate that the structural composition of native HSA without adding ribose consists of 56.0% α-helix (1652 cm^{-1}), 4.4% random coil (1638 cm^{-1}), and 39.6% β-structure (1677 and 1665 cm^{-1}: β-turn (26.2%);, 1630 and 1620 cm^{-1}: β-sheet (13.3%)), which is consistent with the results of other studies [54,55]. The same procedure of fitting was applied to the FTIR spectrum recorded for native HSA after adding ribose at an early stage in the process and yielded the following percentages of secondary structures: 56.5% α-helix (1651 cm^{-1}), 2.6% random coil (1638 cm^{-1}), and 38.9% β-structure (1676 and 1664 cm^{-1}: β-turn (25.7%); 1630 and 1620 cm^{-1}: β-sheet (15.2%)). Both samples exhibited a similar structural composition, suggesting there were no alterations in HSA conformation after the initial addition of ribose.

However, the structural composition of HSA after its reaction with ribose was markedly changed by the amount of ribose added and the length of incubation time, at 37 ± 0.5 ^{o}C and under dark conditions, as shown in Figure 5. It is evident that the α-helix composition of HSA decreased with an increase in ribose concentration and incubation time, whereas the total β-structure and random coil composition increased.

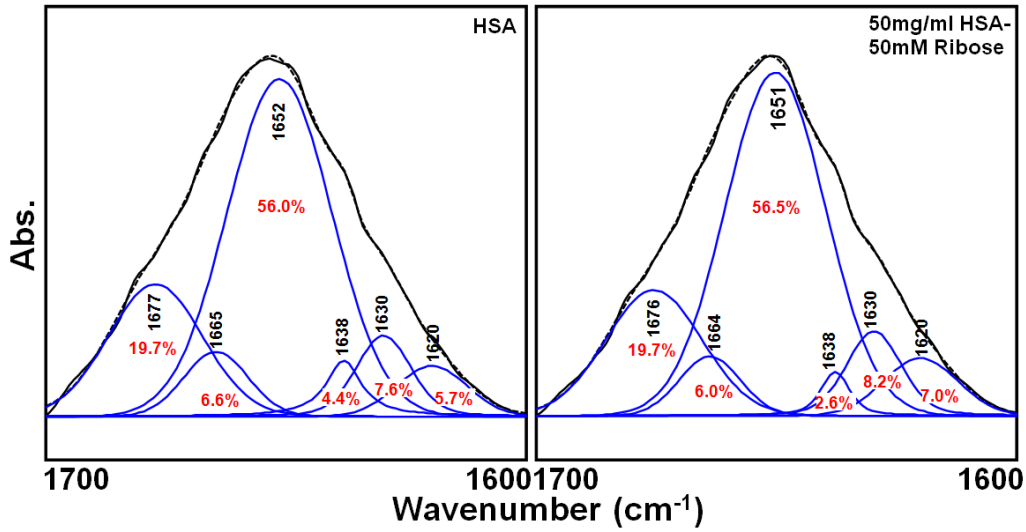

Figure 4. The curve-fitted FTIR amide I band of HSA without or with the addition of ribose at the initial stage.

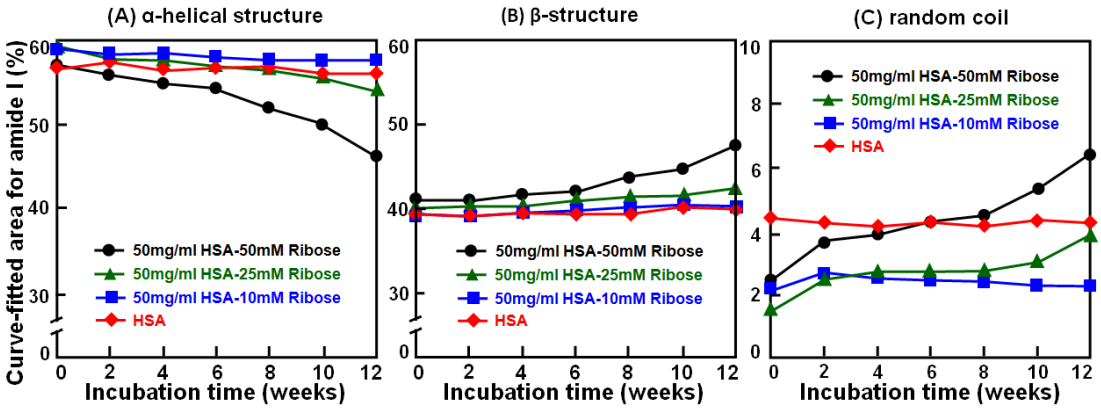

Figure 5. The effect of the concentration of added ribose on the secondary conformational composition of the curve-fitted amide I band of HSA over the course of 12 weeks of incubation. (Each data point represents the mean ± standard deviation (SD) of three independent determinations, but these SD values were too low to show the bars.)

This could be attributed to the loss of helical content due to AGE modification leading to an increase in β-conformation. This is consistent with the results from glycated albumin that showed induced conformational transition from its native α-helical structure to a β-sheeted form [50,56,57], resulting in the formation of protein aggregation and fibrillation [13,27,58,59]. Similar results had also been reported that the interconversion from α-helix conformation to β-sheet structures via a random coil state was found in the other studies [60–62], in which drug or pressure might induce structural alterations in protein conformational transition from α-helix to random coil and to β-sheet structure.

3.4. Ribosylation in the glycation process and protein aggregation

As was previously mentioned, all reducing sugars are capable of participating in glycation reactions, and ribose is more active in the glycation of proteins than other reducing sugars [14–18]. Figure 6 reveals the changes in the ribose consumed in the reaction mixtures during the course of incubation**.** The peak at 1044 cm^{-1} was found in the 1200–1000 cm^{-1} range and corresponded to C-O/C-C stretching vibrations and/or the C-OH/C-C-O bending vibrations of ribose [52]. This peak can be used as an internal marker to estimate the practical participation of ribose in glycation reactions between HSA and ribose, as shown in Figure 6. Since the peak intensity of amide II band at 1542 cm^{-1} did not alter over the course of incubation, the peak intensity of 1044 cm^{-1} was normalized to the peak at 1542 cm^{-1} to determine the consumption of ribose during the reaction [63–65]. It is apparent that the peak intensity ratios of 1044 cm^{-1}/1542 cm^{-1} were markedly decreased with an increase in incubation time up to 4 weeks. After that the changes and the process gradually slowed down. This implies that the glycation process seems to have accelerated over the initial 4-week incubation period and then gradually decreased.

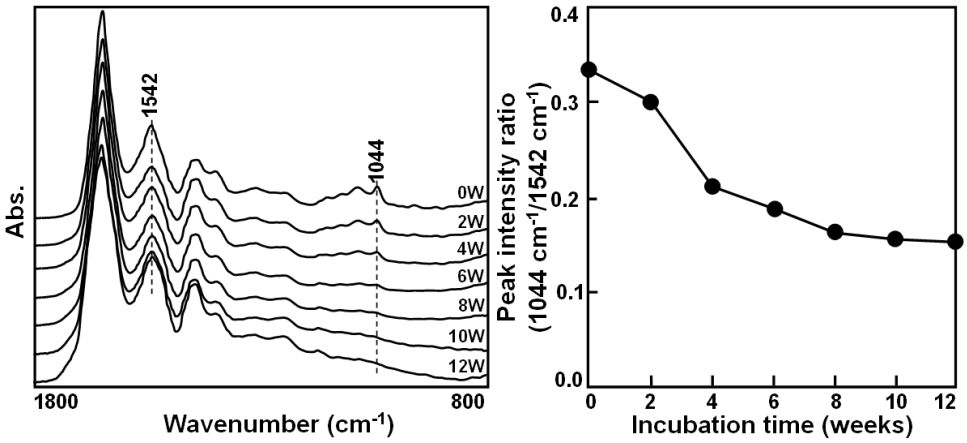

Figure 6. The alterations of ribose consumption for the HSA-ribose reaction mixtures over the course of 12 weeks of incubation.

Nonenzymatic glycation or the Maillard reaction is a process between free amino acid residues of proteins and carbonyl groups of reducing sugars and finally generates AGEs through the formation of a Schiff base and Amadori products [66,67]. AGEs are constructed by a class of irreversible heterogeneous compounds formed by glycation [67] and characterized by a brown color, an auto-fluorescence, and intra- and intermolecular cross-linkings, as shown in Figures 1 and 2. After the application of the FTIR curve-fitting technique to the IR spectra of the HSA–ribose mixtures after glycation, a new curve-fitted FTIR peak at 1710 cm^{-1} was incidentally found after an increase in incubation time, as illustrated in Figure 7. This peak at 1710 cm^{-1} might be due to the carbonyl groups of the complex, irreversible heterogeneous compounds in AGEs such as carboxymethyllysine, pentosidine, pyrraline, carboxyethyllysine and imidanolone [15,68], although we did not attempt to identify these compounds. Obviously, the curve-fitted FTIR peak area at 1710 cm^{-1} increased with incubation time. This clearly shows that the formation of irreversible products and deposition of AGEs gradually occurred in the HSA–ribose mixtures as the incubation time increased.

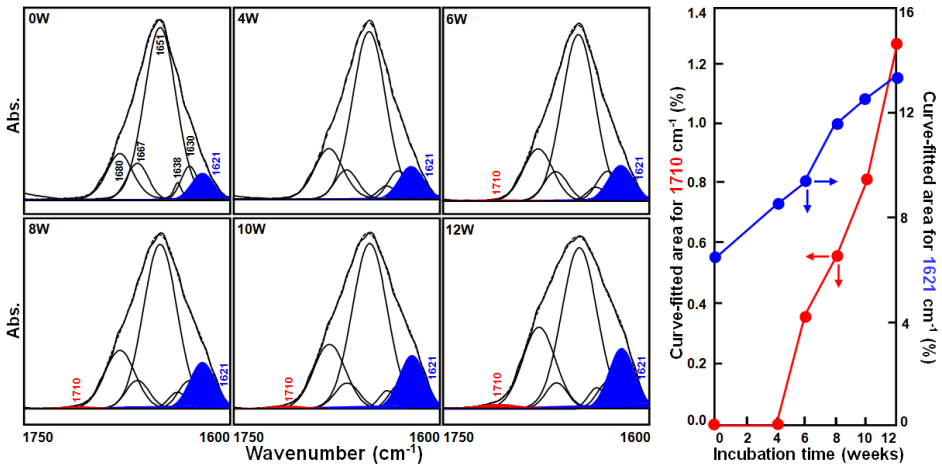

Figure 7. The changes in peak area at 1710 and 1621 cm^{-1} from the curve-fitted amide I band of the HSA-ribose reaction mixtures over the course of 12 weeks of incubation.

FTIR spectroscopy has been used to monitor the aggregation of proteins during various treatments [69,70]. From the curve-fitted FTIR spectra in Figure 7, we can clearly see that an FTIR peak area at 1621 cm^{-1} was enhanced as the incubation time increased. An increased peak area at 1621 cm^{-1} could indicate the formation of intermolecular β-sheets within aggregated protein molecules [71–73]. As the incubation time increases, the gel formation in the reaction mixtures might point toward the aggregation of HSA after ribosylation.

4. Conclusion

In summary, we present the first application of transmission FTIR microspectroscopy with a curve-fitting technique to investigate the secondary conformational changes of HSA after ribosylation. Moreover, the conformational transition in HSA after ribosylation from its native α-helical structure to a β-sheeted form was confirmed. In particular, two unique IR peaks at 1710 and 1620 cm^{-1} from the curve-fitted FTIR spectra, the former possibly indicating the gradual formation of the carbonyl groups of irreversible products of the reaction and the deposition of AGEs in the reaction mixtures of HSA–ribose, and the latter signifying the formation of intermolecular β-sheets within aggregated HSA molecules after ribosylation.

Conflict of Interest

All Authors declare no conflicts of interest in this paper.

References

1. Vanhooren V, Navarrete Santos A, Voutetakis K, et al. (2015) Protein modification and maintenance systems as biomarkers of ageing. *Mech Ageing Dev* 151: 71–84.
2. Uribarri J, Woodruff S, Goodman S, et al. (2010) Advanced glycation end products in foods and a practical guide to their reduction in the diet. *J Am Diet Assoc* 110: 911–916.e12

3. Visentin S, Medana C, Barge A, et al. (2010) Microwave-assisted Maillard reactions for the preparation of advanced glycation end products (AGEs). *Org Biomol Chem* 8: 2473–2477.
4. Horvat S, Jakas A (2014) Peptide and amino acid glycation: new insights into the Maillard reaction. *J Pept Sci* 10: 119–137.
5. Zhang Q, Ames JM, Smith RD, et al. (2009) A perspective on the Maillard reaction and the analysis of protein glycation by mass spectrometry: probing the pathogenesis of chronic disease. *J Proteome Res* 8: 754–769.
6. Dar B, Dar M, Bashir S, et al. (2015) Glycosylated hemoglobin (HbA1c): A biomarker of anti-aging. *Int J Biol Med Res* 6: 5084–5086.
7. Sebekov á K, Somoza V (2007) Dietary advanced glycation endproducts (AGEs) and their health effects--PRO. *Mol Nutr Food Res* 51: 1079–1084.
8. Arasteh A, Farahi S, Habibi-Rezaei M, et al. (2014) Glycated albumin: an overview of the in vitro models of an in vivo potential disease marker. *J Diabetes Metab Disord* 13: 49.
9. Uribarri J, del Castillo MD, de la Maza MP, et al. (2015) Dietary advanced glycation end products and their role in health and disease. *Adv Nutr* 6: 461–473.
10. Takahashi M (2014) Glycation of Proteins. In *Glycoscience: Biology and Medicine*, Endo T, Seeberger PH, Hart GW, Wong CH, Taniguchi N, eds., Springer Japan, pp. 1339–1345
11. Nursten HE (2005) *The Maillard Reaction: Chemistry, Biochemistry, and Implications*. RSC.
12. Laroque D, Inisan C, Berger C, et al. (2008) Kinetic study on the Maillard reaction: Consideration of sugar reactivity. *Food Chem* 111: 1032–1042
13. Sattarahmady N, Moosavi-Movahedi AA, Habibi-Rezaei M, et al. (2008) Detergency effects of nanofibrillar amyloid formation on glycation of human serum albumin. *Carbohydr Res* 343: 2229–2234.
14. Monnier VM (1990) Nonenzymatic glycosylation, the Maillard reaction and the aging process. *J Gerontol* 45: B105–111.
15. Wei Y, Han CS, Zhou J, et al. (2012) D-ribose in glycation and protein aggregation. *Biochim Biophys Acta* 1820: 488–494.
16. Monnier VM, Cerami A (1981) Nonenzymatic browning in vivo: possible process for aging of long-lived proteins. *Science* 211: 491–493.
17. Han C, Lu Y, Wei Y, et al. (2011) D-ribose induces cellular protein glycation and impairs mouse spatial cognition. *PLoS ONE* 6:e24623.
18. Syrov ý I (1994) Glycation of albumin: reaction with glucose, fructose, galactose, ribose or glyceraldehyde measured using four methods. *J Biochem Biophys Methods* 28: 115–121.
19. Kong FL, Cheng W, Chen J, et al. (2011) D-Ribose glycates β(2)-microglobulin to form aggregates with high cytotoxicity through a ROS-mediated pathway. *Chem Biol Interact* 194: 69–78.
20. Khan MS, Dwivedi S, Priyadarshini M, et al. (2013) Ribosylation of bovine serum albumin induces ROS accumulation and cell death in cancer line (MCF-7). *Eur Biophys J* 42: 811–818.
21. Iannuzzi C, Maritato R, Irace G, et al. (2013) Glycation accelerates fibrillization of the amyloidogenic W7FW14F apomyoglobin. *PLoS ONE* 8: e80768.
22. Adrover M, Mari ño L, Sanchis P, et al. (2014) Mechanistic insights in glycation-induced protein aggregation. *Biomacromolecules* 15: 3449–3462.
23. Liu J, Ru Q, Ding Y (2012) Glycation a promising method for food protein modification: Physicochemical properties and structure, a review. *Food Res Int* 49: 170–183.

24. Wei Y, Chen L, Chen J, et al. (2009) Rapid glycation with D-ribose induces globular amyloid-like aggregations of BSA with high cytotoxicity to SH-SY5Y cells. *BMC Cell Biol* 10: 10.
25. Kragh-Hansen U, Chuang VT, Otagiri M (2002) Practical aspects of the ligand-binding and enzymatic properties of human serum albumin. *Biol Pharm Bull* 25: 695–704.
26. Santra MK, Banerjee A, Krishnakumar SS, et al. (2004) Multiple-probe analysis of folding and unfolding pathways of human serum albumin. Evidence for a framework mechanism of folding. *Eur J Biochem* 271: 1789–1797.
27. Anguizola J, Matsuda R, Barnaby OS, et al. (2013) Review: Glycation of human serum albumin. *Clin Chim Acta* 2013; 425: 64–76.
28. Singha Roy A, Ghosh P, Dasgupta S (2015) Glycation of human serum albumin alters its binding efficacy towards the dietary polyphenols: A comparative approach. *J Biomol Struct Dyn* Oct 7:1–46. [In press].
29. Peters T (1996) All about Albumin. Biochemistry, Genetics, and Medical Applications. Academic Press, San Diego, CA.
30. Khan MW, Rasheed Z, Khan WA, et al. (2007) Biochemical, biophysical, and thermodynamic analysis of in vitro glycated human serum albumin. *Biochemistry (Mosc)* 72: 146–152.
31. Yang F, Zhang Y, Liang H (2014) Interactive association of drugs binding to human serum albumin. *Int J Mol Sci* 15: 3580–3595.
32. Lin SY, Wei YS, Li MJ, et al (2004). Effect of ethanol or/and captopril on the secondary structure of human serum albumin before and after protein binding. *Eur J Pharm Biopharm* 57: 457–464.
33. Lin SY, Wei YS, Li MJ (2004) Ethanol or/and captopril-induced precipitation and secondary conformational changes of human serum albumin. *Spectrochim Acta A* 60: 3107–3111.
34. Li MJ, Lin SY (2005) Vibrational spectroscopic studies on the disulfide formation and secondary conformational changes of captopril-HSA mixture after UV-B irradiation. *Photochem Photobiol* 81: 1404–1410.
35. Sadowska-Bartosz I, Galiniak S, Bartosz G (2014) Kinetics of glycoxidation of bovine serum albumin by glucose, fructose and ribose and its prevention by food components. *Molecules* 19: 18828–18849.
36. Kosaraju SL, Weerakkody R, Augustin MA (2010) Chitosan-glucose conjugates: influence of extent of Maillard reaction on antioxidant properties. *J Agric Food Chem* 58: 12449–12455.
37. Ajandouz EH, Tchiakpe LS, Ore FD, et al. (2001) Effects of pH on caramelization and Maillard reaction kinetics in fructose-lysine model systems. *J Food Sci* 66: 926–931.
38. Monacelli F, Storace D, D'Arrigo C, et al. (2013) Structural alterations of human serum albumin caused by glycative and oxidative stressors revealed by circular dichroism analysis. *Int J Mol Sci* 14: 10694–10709.
39. Lee TH, Cheng WT, Lin SY (2010) Thermal stability and conformational structure of salmon calcitonin in the solid and liquid states. *Biopolymers* 93: 200–207.
40. Ledesma-Osuna AI, Ramos-Clamont G, Vazquez-Moreno L (2008) Characterization of bovine serum albumin glycated with glucose, galactose and lactose. *Acta Biochim Pol* 55: 491–497.
41. Sompong W, Meeprom A, Cheng H, et al. (2013) A comparative study of ferulic acid on different monosaccharide-mediated protein glycation and oxidative damage in bovine serum albumin. *Molecules* 18: 13886–13903.

42. Wu CH, Huang SM, Lin JA, et al. (2011) Inhibition of advanced glycation endproduct formation by foodstuffs. *Food Funct* 2: 224–234.
43. Kato Y, Matsuda T, Kato N, et al. (1989) Maillard reaction of disaccharides with protein: suppressive effect of nonreducing end pyranoside groups on browning and protein polymerization. *J Agric Food Chem* 37: 1077–1081.
44. Suárez G, Rajaram R, Oronsky AL, et al. (1989). Nonenzymatic glycation of bovine serum albumin by fructose (fructation). Comparison with the Maillard reaction initiated by glucose. *J Biol Chem* 264: 3674–3679.
45. McPherson JD, Shilton BH, Walton DJ (1988) Role of fructose in glycation and cross-linking of proteins. *Biochemistry* 27: 1901–1907.
46. Siddiqui AA, Sohail A, Bhat SA, et al. (2015). Non-enzymatic glycation of almond cystatin leads to conformational changes and altered activity. *Protein Pept Lett* 22: 449–459.
47. Awasthi S, Murugan NA, Saraswathi NT (2015) Advanced glycation end products modulate structure and drug binding properties of albumin. *Mol Pharmaceutics* 12: 3312–3322.
48. Bouma B, Kroon-Batenburg LM, Wu YP, et al. (2003) Glycation induces formation of amyloid cross-beta structure in albumin. *J Biol Chem* 278: 41810–41819.
49. Khajehpour M, Dashnau JL, Vanderkooi JM (2006) Infrared spectroscopy used to evaluate glycosylation of proteins. *Anal Biochem* 348: 40–48.
50. GhoshMoulick R, Bhattacharya J, Roy S, et al. (2007). Compensatory secondary structure alterations in protein glycation. *Biochim Biophys Acta* 1774: 233–242.
51. Yang H, Yang S, Kong J, et al. (2015). Obtaining information about protein secondary structures in aqueous solution using Fourier transform IR spectroscopy. *Nat Protoc* 10: 382–396.
52. Roy R, Boskey A, Bonassar LJ (2010) Processing of type I collagen gels using nonenzymatic glycation. *J Biomed Mater Res A* 93: 843–851.
53. Haris PI (2013) Probing protein-protein interaction in biomembranes using Fourier transform infrared spectroscopy. *Biochim Biophys Acta* 1828: 2265–2271.
54. Neault JF, Tajmir-Riahi HA (1998) Interaction of cisplatin with human serum albumin. Drug binding mode and protein secondary structure, *Biochim. Biophys Acta* 1384: 153–159.
55. Bramanti E, Benedetti E (1996) Determination of the secondary structure of isomeric forms of human serum albumin by a particular frequency deconvolution procedure applied to Fourier transform IR analysis. *Biopolymers* 38: 639–653.
56. Zsila F (2013) Subdomain IB is the third major drug binding region of human serum albumin: toward the three-sites model. *Mol Pharmaceutics* 10: 1668–1682.
57. Awasthi S, Murugan NA, Saraswathi NT (2015) Advanced glycation end products modulate structure and drug binding properties of albumin. *Mol Pharmaceutics* 12: 3312–3322.
58. Khan TA, Saleemuddin M, Naeem A (2011) Partially folded glycated state of human serum albumin tends to aggregate. *Int J Pept Res Ther* 17: 271–279.
59. Oliveira LM, Lages A, Gomes RA, et al. (2011) Insulin glycation by methylglyoxal results in native-like aggregation and inhibition of fibril formation. *BMC Biochem* 5; 12:41.
60. Lin SY, Chu HL, Wei YS (2002) Pressure-induced transformation of alpha-helix to beta-sheet in the secondary structures of amyloid beta (1–40) peptide exacerbated by temperature. *J Biomol Struct Dyn* 19: 619–625.
61. Ding F, Borreguero JM, Buldyrey SV, et al. (2003) Mechanism for the alpha-helix to beta-hairpin transition. *Proteins* 53: 220–228.

62. Garip S, Yapici E, Ozek NS, et al. (2010) Evaluation and discrimination of simvastatin-induced structural alterations in proteins of different rat tissues by FTIR spectroscopy and neural network analysis. *Analyst* 135: 3233–3241.
63. Yano K, Ohoshima S, Shimizu Y, et al. (1996) Evaluation of glycogen level in human lung carcinoma tissues by an infrared spectroscopic method. *Cancer Lett* 110: 29–34.
64. Podshyvalov A, Sahu RK, Mark S, et al. (2005) Distinction of cervical cancer biopsies by use of infrared microspectroscopy and probabilistic neural networks. *Appl Opt* 44: 3725–3734.
65. Colagar AH, Chaichi MJ, Khadjvand T (2011) Fourier transform infrared microspectroscopy as a diagnostic tool for distinguishing between normal and malignant human gastric tissue. *J Biosci* 36: 669–677.
66. Nagai R, Shirakawa J, Fujiwara Y, et al. (2014) Detection of AGEs as markers for carbohydrate metabolism and protein denaturation. *J Clin Biochem Nutr* 55: 1–6.
67. Rondeau P, Bourdon E (2011) The glycation of albumin: structural and functional impacts. *Biochimie* 93: 645–658.
68. Basta G, Schmidt AM, De Caterina R (2004) Advanced glycation end products and vascular inflammation: implications for accelerated atherosclerosis in diabetes. *Cardiovasc Res* 63: 582–592.
69. Shivu B, Seshadri S, Li J, et al. (2013) Distinct β-sheet structure in protein aggregates determined by ATR-FTIR spectroscopy. *Biochemistry* 52: 5176–5183.
70. Natalello A, Doglia SM (2015) Insoluble protein assemblies characterized by fourier transform infrared spectroscopy. *Methods Mol Biol* 1258: 347–369.
71. Clark AH, Saunderson DH, Suggett A (1981) Infrared and laser-Raman spectroscopic studies of thermally-induced globular protein gels. *Int J Pept Protein Res* 17: 353–364.
72. Ruggeri FS, Longo G, Faggiano S, et al. (2015) Infrared nanospectroscopy characterization of oligomeric and fibrillar aggregates during amyloid formation. *Nat Commun* 6: 7831.
73. Miller LM, Bourassa MW, Smith RJ (2013) FTIR spectroscopic imaging of protein aggregation in living cells. *Biochim Biophys Acta* 1828: 2339–2346.

AIMS Press